Food Chemistry: X 21 (2024) 101207

Contents lists available at ScienceDirect

Food Chemistry: X

journal homepage: www.sciencedirect.com/journal/food-chemistry-x

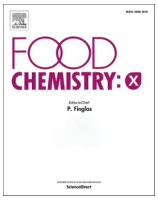

Food-grade silica-loaded gallic acid nanocomposites: Synthesis and mechanism for enhancing water-based biological activity

Huizhen Feng [a], Long Jiao [a,*], Xiaoye Zhang [b,*], Soottawat Benjakul [c], Bin Zhang [a,d]

[a] Key Laboratory of Health Risk Factors for Seafood of Zhejiang Province, College of Food Science and Pharmacy, Zhejiang Ocean University, PR China
[b] School of Naval Architecture and Maritime, Zhejiang Ocean University, PR China
[c] International Center of Excellence in Seafood Science and Innovation, Faculty of Agro-Industry, Prince of Songkla University, Thailand
[d] Pisa Marine Graduate School, Zhejiang Ocean University, PR China

ARTICLE INFO

Keywords:
Gallic acid
Food-grade silica
Nanocomposite
Water-based biological activity

ABSTRACT

As the low water solubility of gallic acid (GA), its biological activities such as water-based antioxidant effect may be greatly reduced. Therefore, GA-loaded nanocomposites (F-SiO_2@GA) with high water solubility were synthesized via solvent evaporation using food-grade silica (F-SiO_2) as carriers in this work. The assessment of antioxidant capacity revealed that F-SiO_2@GA exhibited considerably greater free-radical scavenging ability than free GA and the physical mixture of F-SiO_2 and GA. In the photooxidation experiment of food-grade gardenia yellow pigment (GYP), F-SiO_2@GA showed a notable antioxidant effect on GYP solution. Additionally, in the storage experiment on chilled whiteleg shrimp (*Litopenaeus vannamei*) treated with F-SiO_2@GA, pH, total volatile basic nitrogen (TVBN), and thiobarbituric acid reactive substance (TBARS) values were effectively inhibited. In conclusion, the internal encapsulation of GA effectively prevented the self-aggregation phenomenon, thereby facilitating the exposure of its active phenolic hydroxyl group and significantly enhancing its water-based biological activity.

1. Introduction

Antioxidants play a pivotal role in food preservation by effectively retarding or inhibiting food oxidation, thereby enhancing food stability and extending shelf life (Huang et al., 2023). Propyl gallate, butylated hydroxyanisole, butylated hydroxytoluene, and tertiary butylhydroquinone are commonly used food antioxidants. However, these synthetic antioxidants have unfavorable consumer acceptance due to concerns regarding their potential toxicity (Othón-Díaz et al., 2023). Consequently, an inclination toward the utilization of natural antioxidants in lieu of their synthetic counterparts for food preservation is emerging (Petcu et al., 2023).

Polyphenols are natural antioxidants with diverse biological activities (Zhao et al., 2023). GA (3,4,5-trihydroxybenzoic acid) is a representative natural phenolic acid that is widely distributed in various fruits and medicinal plants (Li et al., 2023). It possesses various biological activities, including antioxidant, antibacterial, and anti-inflammatory activities, and has been authorized as a safe food additive by the drug committees of many countries (Wianowska & Olszowy-Tomczyk, 2023). The active phenol hydroxyl group in GA molecule can act as a hydrogen donor to eliminate free radicals by providing hydrogen atoms, thus inhibiting lipid and protein oxidation (Wang et al., 2022). However, the aromatic ring structure in GA molecule is prone to π–π stacking in aqueous solutions (Fig. 1) (Song et al., 2021). This behavior reduces the water solubility of GA at room temperature and low temperature and further limits the hydrogen supply capacity of GA molecules, eventually reducing the antioxidant activity in water-based environments considerably (Pinho et al., 2015). Additionally, the antioxidant ability of GA is highly dose-dependent. Hence, the antioxidant applications of GA in water-based food systems are severely limited (Dong et al., 2022).

Nanocarriers have recently garnered considerable attention because of their ability to enhance the water solubility and bioavailability of insoluble molecules, making them increasingly prevalent in the realm of food additives and packaging (Li et al., 2022a; Zhang et al., 2023). Among various nanomaterials, silica nanoparticles (SiO_2 NPs) have high water solubility, specific surface area, and thermodynamic stability as well as low biotoxicity. These characteristics confer SiO_2 NP carrier nanomaterials with great application potential (Cui et al., 2023). Numerous theoretical studies have been conducted to enhance the bioavailability of bioactive molecules, such as curcumin, GA, and

* Corresponding authors at: No.1, Haida South Road, Lincheng Changzhi Island, Zhoushan, Zhejiang province 316022, PR China.
E-mail addresses: jiaolong502@zjou.edu.cn (L. Jiao), 2022096@zjou.edu.cn (X. Zhang).

https://doi.org/10.1016/j.fochx.2024.101207
Received 4 November 2023; Received in revised form 2 January 2024; Accepted 4 February 2024
Available online 8 February 2024

catechol, by loading them into mesoporous silica materials (Rahaman et al., 2023). However, limited research has been conducted on the synthesis of edible F-SiO_2 loaded with GA nanocomposites and their applications as water-based antioxidants.

In this study, we prepared F-SiO_2–loaded GA nanocomposites to improve the water solubility and water-based antioxidant activity of GA. F-SiO_2–loaded GA nanocomposites were prepared by using two different loading methods, namely, solvent evaporation and slow adsorption, to obtain distinct loading forms of GA. These novel nanocomposites were characterized based on microscopic observation, spectral properties, and stability. Moreover, their water-based antioxidant activity was evaluated. Finally, the antioxidant and preservative effects of the nanocomposites on gardenia yellow pigment (GYP) and fresh L. *vannamei* were investigated. This work will provide a new idea and solution strategy for the practical application of GA as a water-based food antioxidant.

2. Materials and methods

2.1. Chemical reagents

F-SiO_2 was provided by Hubei Huifu Nanomateral Co. Ltd. (Yichang, China). GA (98 %) was obtained from Energy-Chemical (Shanghai, China). Absolute alcohol was procured from Sinopharm Chemical Reagent Co. Ltd. (Suzhou, China). The free radical assay kits used for determination of 1,1-diphenyl-2-picrylhydrazyl free radical (DPPH•), hydroxy free radical (•OH^-), superoxide anion free radical ($O_2^{\bullet-}$) were purchased from Nanjing Jiancheng Biotechnology Co. Ltd. (Nanjing, China). GYP (98 %) was purchased from Henan Zhongda Bioengineering Co. Ltd. (Luohe, China). All the chemical reagents were all of analytical grade. Ultrapure deionized water from a Milli-Q ultrapure system (UPR-I-5TNZP, Sichuan UPR, China) was used for all analysis, separation and purification steps.

2.2. Preparation of food-grade silica-loaded gallic acid nanocomposites

A solvent evaporation method with some modifications was utilized to prepare food-grade silica-loaded gallic acid nanocomposite (He et al., 2017). Briefly, F-SiO_2 (500 mg) was mixed with GA (500 mg) in a round-bottomed flask containing 20 mL of anhydrous alcohol and then reacted for 6 h at 50 °C with stirring. After the reaction, ethanol was removed from the mixture using a rotary evaporator. The mixture was then washed three times with anhydrous ethanol. Finally, the nanocomposite labeled as F-SiO_2@GA was dried in a vacuum drying oven. Meanwhile, an adsorption method with some modifications was utilized to prepare another type of food-grade silica-loaded gallic acid nanocomposite (Eren et al., 2016). Further, F-SiO_2 (500 mg) was mixed with GA (500 mg) in a round-bottomed flask containing 20 mL of anhydrous alcohol and reacted for 24 h at 50 °C with stirring. After the reaction, the hybrid material was collected through direct centrifugation and washed three times with anhydrous ethanol. Finally, the nanocomposite labeled as GA@F-SiO_2 was collected again and dried in a vacuum drying oven.

The physical mixture comprising equal mass ratios of F-SiO_2 and GA was denoted as F-SiO_2/GA.

2.3. Standard curve plotting and loading capacity determination

The maximum UV absorption wavelength of the GA solution was measured using a UV–Vis spectrophotometer (U-2800, HITACHI, Japan) at 217 nm. Subsequently, concentration gradient sample solutions were measured at 217 nm to establish the standard curve for GA concentration measurement ($R^2 = 0.9997$; $C = 0.1327A + 0.002$).

The loading capacity of GA was determined by preparing aqueous solutions of F-SiO_2@GA and F-SiO_2/GA with specific concentrations and calculated using Eq. (1) as follows:

$$Loading\ \ capacity(\%) = \frac{C_2}{C_1} \times 100 \quad (1)$$

where C_1 is the concentration of the sample, and C_2 is the concentration of GA in the sample.

2.4. Characterization

2.4.1. Scanning electron microscope (SEM) analysis

Dry samples were fixed to a mental support and sputtered with a coating of gold under vacuum. SEM (Sigma 300, Zeiss, Germany) was used to examine the sample's morphology at an accelerating voltage of 15.0 kV.

2.4.2. Fourier-transform infrared (FT-IR) spectroscopy analysis

The dried samples were co-ground with KBr powder and tableted. The infrared absorption properties of the samples were examined using FT-IR spectrometer (Nicolet iS 10, Thermo fisher, USA). The value of resolution was 4 cm^{-1}, with 32 scans spanning the wavenumber range of 400–4000 cm^{-1}.

2.4.3. UV–vis spectroscopy analysis

The UV–Vis spectrums of the aqueous sample solutions (15 μg/mL) were scanned by a UV–Vis absorption and fluorescence spectrometer in one (Duetta, HORIBA, Japan) from 200–600 nm.

2.4.4. Evaluation of thermal stability

The thermal stability of the solid samples was evaluated by differential scanning calorimetry (TA, Netzsch, Germany). The sample (10.0 mg) was place in aluminum pans. Thermal analysis procedure from 30℃ to 350℃ at rate of 10℃/min under a nitrogen flow of 20 mL/min.

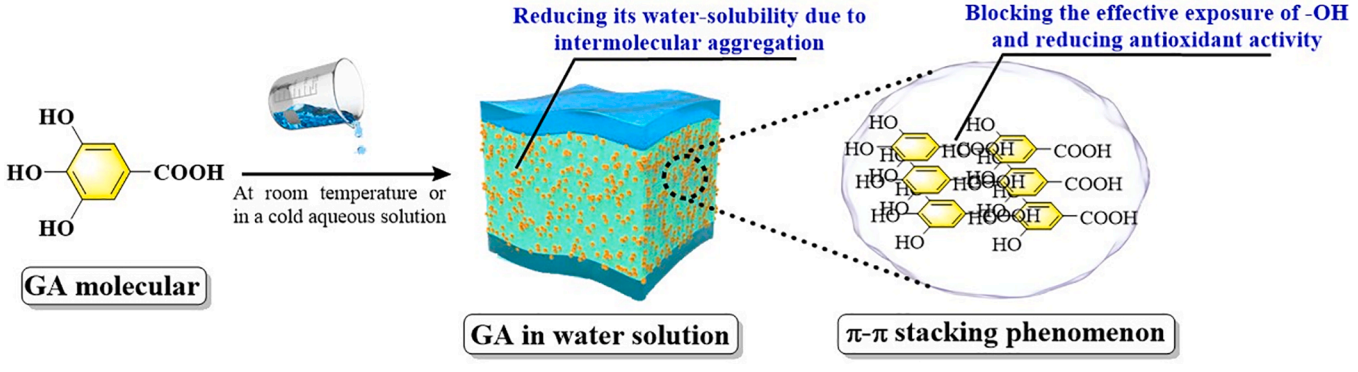

Fig. 1. Molecular structure of GA and its aggregation behavior in aqueous solution.

2.4.5. Evaluation of saturated solubility

The solubility of the samples was investigated using reported methods with some modifications (Chen et al., 2020). The saturated solution was prepared by dissolving a specific quantity of the samples in a small volume of distilled water. Sub the resulting solution underwent magnetic stirring for 5 min and was subsequently filtered using 0.22 μm membrane. Following filtration, 0.2 mL of filtrate was transferred into a dry sample bottle, which was then subjected to drying and subsequent weighing. The solubility was calculated using Eq. (2) as follows:

$$Solubility(mg/mL) = \frac{m_2 - m_1}{0.2mL} \quad (2)$$

where m_1 is weight of sample bottle, and m_2 is the total weight of bottle and sample after drying.

2.4.6. Dispersion stability

The samples were dispersed in ultrapure water (12 mg/mL, calculated on the basis of GA content) using ultrasonic treatment to investigate their long-term dispersion stability (0–12 d) in aqueous solutions.

2.5. Antioxidant activity measurements

The sample (GA, F-SiO_2@GA, and F-SiO_2/GA) was configured with a saturated aqueous solution and then the supernatant was filtered with a 0.22 μm nylon membrane. Afterward, the filtrate was diluted to the test concentration with ultrapure water. Subsequently, the radical scavenging activity of the samples was estimated using an assay kit for free-radical scavenging capacity (Nanjing Jiancheng Bioengineering Institute, Nanjing, China).

2.6. Stability determination of GYP

The retention rate of GYP was investigated by using reported methods with slight modifications (Wu et al., 2022). Briefly, 0.1 g of GYP was dissolved in 100 mL of NaH_2PO_4/NaOH buffer solution (0.01 M, pH = 5.5). Subsequently, 0.02 g of GA, F-SiO_2/GA, or F-SiO_2@GA (calculated based on GA content) was added to 20 mL of GYP solutions (0.1 % w/v). The mixture was stirred for 5 min and filtered through a 0.22 μm membrane. Next, the filtrate was diluted to 130 μg/mL with buffer. A series of transparent sample bottles were filled with 15 mL of each mixed solution and closed with screw caps. All solutions were exposed to natural light for 10 h to accelerate the potential degradation of GYP. The solutions were then collected every 1 h for further analysis. The stability of GYP was evaluated by measuring the UV–Vis absorbance values at 440 nm, and the GYP retention rate was calculated using Eq. (3).

$$Retention rate of GYP(\%) = \frac{A_1}{A_0} \times 100 \quad (3)$$

where A_1 is the absorbance of GYP, and A_0 is the initial absorbance of GYP.

2.7. Experiment of fresh shrimp preservation

Aqueous solutions of GA, F-SiO_2/GA, and F-SiO_2@GA were prepared with a final concentration of 5 mmol/L (based on GA content). Fresh L. *vannamei* (~20 g) were purchased from a local market in Zhoushan, China. The shrimp were inactivated using ice slurry and rinsed with sterile distilled water. The shrimp were then randomly allocated into four groups and subjected to the following treatments: Control group (1) (CK)- immersion in deionized water for 30 min. Experimental group (2) (GA treatment), group (3) (F-SiO_2/GA treatment), and group (4) (F-SiO_2@GA treatment)- 30 min of immersion in the sample solution. After soaking, the solution was drained for 5 min at 4℃. Shrimp samples from each group were then carefully packaged in polyethylene trays and refrigerated at 4℃ to ensure optimal quality evaluation.

2.7.1. pH measurement

A 2.0 g sample of minced shrimp was homogenized with 18 mL of distilled water for 1 min and then soaked at 4 °C for 30 min. Subsequently, the pH of the filtrate was determined at room temperature.

2.7.2. TVBN measurement

A 10.0 g sample of chopped shrimp was homogenized with 75 mL of distilled water and impregnated for 30 min in a distillation tube. Subsequently, 1.0 g of MgO was added to the distillation tube, and five drops of the mixed indicator (bromocresol green–methyl red ethanol solution) were placed in a conical flask. A nitrogen determinator (KDN-520, BANGYES, China) was connected to the distillation tube and conical flask. The contents of the conical flask were titrated with hydrochloric acid (0.01 M) after distillation until their color changed from blue to purple-red. TVBN value was determined by using Eq. (4) as follows:

$$TVBN(mg/100g) = \frac{(V_1 - V_2) \times c \times 14}{m} \times 100 \quad (4)$$

where V_1 is the volume of HCl used by the sample (mL), V_2 is the volume of HCl used by the blank (mL), c is the HCl concentration used in this experiment (0.1 M), and m is the mass of the samples (g).

2.7.3. Thiobarbituric acid reactive substance (TBARS) measurements

TBARS in shrimp meat was determined according to Abbasi (2023). The TBARS value was expressed as mg MDA/kg shrimp meat.

2.8. Cytotoxicity of the nanocomposites

Raw264.7 macrophages cells (KeyGEN BioTECH, Nanjing, China) were used to evaluate the cytotoxicity of GA, F-SiO_2/GA, and F-SiO_2@GA through methyl tetrazolium (MTT) method. Briefly, the cells were seeded in 96-well plates at a density of 5×10^4 per well and were maintained in DMEM containing 10 % fetal bovine serum, supplemented with 100 U/mL penicillin and 100 μg/mL streptomycin, and incubated at 37 °C in a humidified cell culture incubator with 5 % CO_2 atmosphere for 24 h. The cells were washed three times with PBS, and 200 μL sample solution with the concentration of 0, 0.05, 0.10, 0.25, and 0.5 mg/mL (GA content) was added to each well for incubation. After being incubate for another 12 h, the cells were subjected to MTT assay by microplate reader (Multiskan FC, Thermo scientific, USA).

2.9. Data analysis

The statistical evaluation was conducted using SPSS 13.0. The significant differences between different treatments were determined using the Duncan's test method, and a *P*-value under 0.05 showed that the means were significantly distinct. The nonlinear regression model of GraphPad Prism 9.0 was used for obtaining the IC_{50} values. Results were provided as the mean and standard deviation (SD) of three parallel experimental measurements.

3. Results and discussion

3.1. Characterization of the hybrid material

3.1.1. SEM micrographs

SEM was utilized to investigate the surface morphology of the prepared nanocomposites (Fig. 2). As depicted in the partially enlarged image in Fig. 2A, F-SiO_2 nanoparticles exhibited regular spherical particles and a uniform distribution state. Two distinct solid components were clearly observed in Fig. 2B, with F-SiO_2 marked by the red arrow and pure GA crystals marked by the yellow arrow. Notably, solvent evaporation yielded F-SiO_2@GA with a uniform distribution that did not

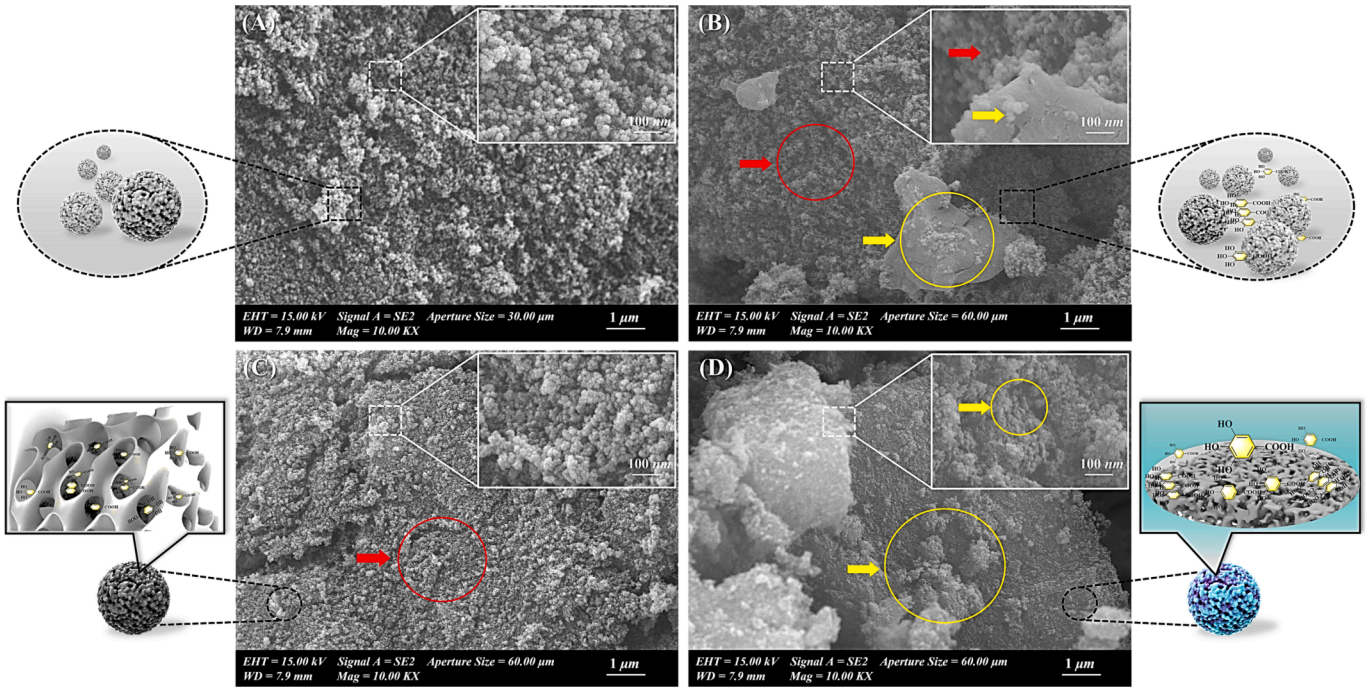

Fig. 2. SEM images of solid samples (A) F-SiO_2, (B) F-SiO_2/GA, (C) F-SiO_2@GA, and (D) GA@F-SiO_2.

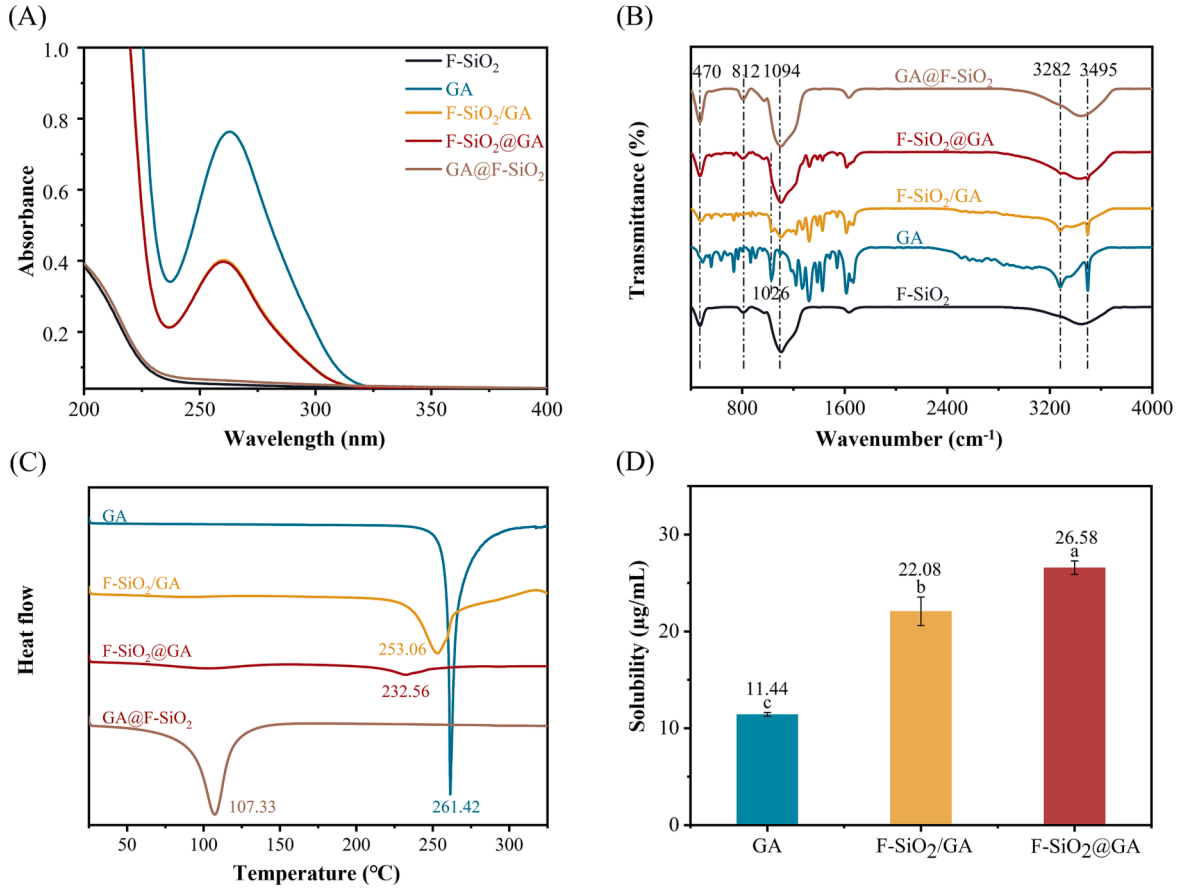

Fig. 3. (A) UV–Vis and (B) FT-IR spectra of F-SiO_2, GA, F-SiO_2/GA, F-SiO_2@GA, and GA@F-SiO_2. (C) DSC curves of solid samples GA, F-SiO_2/GA, F-SiO_2@GA, and GA@F-SiO_2. (D) The solubility of GA, F-SiO_2/GA, F-SiO_2@GA in water. Data are expressed as the mean of three different measurements ± SD.

have the typical crystal structure of GA (Fig. 2C). Therefore, the majority of GA molecules were speculated to have loaded within silica pores, with only a small amount existing in interparticle gaps. In contrast to sample F-SiO_2/GA, F-SiO_2@GA did not show agglomeration. The lack of agglomeration was beneficial for maintaining the optimal hydrophilicity of F-SiO_2. No remarkable difference in surface states was observed between F-SiO_2@GA and F-SiO_2. As presented in Fig. 2D, typical crystal particles of GA appeared on the surface of GA@F-SiO_2 and almost completely masked the typical morphology of F-SiO_2. Therefore, GA@F-SiO_2 was prepared via the adsorption method, resulting in the surface adsorption of GA rather than its internal incorporation.

3.1.2. Spectroscopy analysis

Next, the UV–Vis spectra of the samples were measured (Fig. 3A). GA, F-SiO_2/GA, and F-SiO_2@GA exhibited remarkable GA absorption peaks near 263 nm caused by the π-system of the benzene ring (Zhang et al., 2020). Calculation revealed that the GA contents of F-SiO_2/GA, F-SiO_2@GA, and GA@F-SiO_2 were 50 %, 46.78 %, and 1.44 %, respectively. Furthermore, consistent with the order of GA content, the absorption intensities of the samples decreased in the order of GA > F-SiO_2/GA > F-SiO_2@GA > GA@F-SiO_2 > F-SiO_2. The samples were characterized based on their FT-IR spectra (Fig. 3B) to further analyze the weak interaction between GA and F-SiO_2. GA had the following infrared characteristic peaks: –OH stretching of the benzene ring at 3495 and 3282 cm^{-1}, C—O stretching of carboxy groups at 1634 cm^{-1}, C—C stretching of the aromatic ring at 1481 and 1612 cm^{-1}, C—O/C—C stretching vibrations at 1200–1300 cm^{-1}, and aromatic C—H deformation at 1026 cm^{-1} (Liu, 2021a). F-SiO_2 exhibited the following major characteristic peaks: the symmetrical stretching and bending vibration peaks of Si–O–Si at 812 and 470 cm^{-1}, respectively; the bending vibration peak of Si–OH at 970 cm^{-1}; and the asymmetric contraction vibration peak of Si–O–Si at 1094 cm^{-1} (Hu et al., 2022). The characteristic peaks of GA were observed in the spectra of F-SiO_2/GA. Moreover, the infrared characteristic peaks of F-SiO_2 were partially obscured by GA. This result indicated that F-SiO_2/GA was simply a physical mixture (Liu et al., 2021b). After solvent evaporation, the characteristic peak (1026 cm^{-1}) of GA disappeared from the spectrum of F-SiO_2@GA, indicating that GA was coated with F-SiO_2. This finding, along with the SEM observations above, demonstrated that GA in F-SiO_2@GA was loaded into F-SiO_2. Notably, almost no characteristic peaks of GA were found in GA@F-SiO_2. The loading measurement results illustrated that GA was poorly coated or adsorbed via the adsorption method, limiting its practical application as an antioxidant.

3.1.3. DSC analysis

Further, the thermal stability of the solid samples was evaluated through DSC (Fig. 3C). GA presented a typical sharp melting endothermic peak at 261.42 °C that was associated with the melting point of GA (252 °C) and indicated an anhydrous crystalline state (Aydogdu et al., 2019). The DSC curve of F-SiO_2/GA showed the superimposed heating distributions of GA and F-SiO_2. Given that F-SiO_2 lacked an endothermic peak and was in a noncrystalline state, F-SiO_2/GA had only one melting endothermic peak. In contrast, F-SiO_2@GA lacked a remarkable endothermic peak, indicating that GA had been completely dispersed in F-SiO_2 through solvent evaporation and existed in an amorphous state. Compared with the crystalline state, the amorphous state had a lower lattice energy, thereby showing improved bioavailability and dissolution rates. However, the melting point of GA@F-SiO_2 decreased sharply, indicating that the crystalline transition greatly reduced thermal stability. This result might be due to the reduction in the melting point caused by the increase in the free energy of GA adsorbed on the surface of F-SiO_2. Notably, GA@F-SiO_2 would require a considerably higher dosage than F-SiO_2@GA to obtain the same biological activity as F-SiO_2@GA due to its low GA content (1.44 %). The utilization of GA@F-SiO_2 at high doses as a food antioxidant may potentially exacerbate its inherent toxicity. Consequently, further experimental investigations will not incorporate GA@F-SiO_2.

3.1.4. Saturated solubility evaluation

Poor water solubility may result in a substantial reduction in the water-based antioxidant activity and bioavailability of antioxidants (Li et al., 2022a). The water solubility of GA, F-SiO_2/GA, and F-SiO_2@GA was evaluated. Fig. 3D showed that F-SiO_2@GA exhibited good solubility in water (26.58 ± 0.69 μg/mL) and was considerably higher than that of GA (11.44 ± 0.19 μg/mL) and F-SiO_2/GA (22.08 ± 1.47 μg/mL). The solubility of F-SiO_2@GA increased by 232 % and 120 %, respectively, compared with that of GA and F-SiO_2/GA. In F-SiO_2@GA, the increase in water solubility could be attributed to the loading of GA into F-SiO_2. This phenomenon preserved the hydrophilic surface properties of F-SiO_2. However, in F-SiO_2/GA, the mechanical interaction of GA with F-SiO_2 was restricted to the surface of F-SiO_2 and the nonuniform adherence of GA to the surface of F-SiO_2 resulted in a reduction in water solubility. Therefore, adopting F-SiO_2 as a carrier and employing solvent evaporation could effectively improve the solubility of GA.

3.1.5. Dispersion stability

The long-term dispersion stability of F-SiO_2@GA in water was evaluated to further validate its potential as a water-based antioxidant. GA had poor water solubility. And particles that were poorly dispersed in the solvent were prone to collision, resulting in the formation of large agglomerates. Fig. 4 showed that GA underwent considerable precipitation in a short time, indicating that it has poor dispersion stability in aqueous solutions. Given that F-SiO_2/GA was a mechanical mixture of GA and hydrophilic F-SiO_2, the white precipitate was identified as undissolved GA. Moreover, the dispersion stability of GA and F-SiO_2/GA gradually deteriorated with increasing standing time due to intermolecular aggregation caused by the π–π accumulation of the aromatic ring structures in GA molecules. F-SiO_2@GA showed no obvious precipitation after 12 days of storage, thereby demonstrating its excellent water solubility and dispersion stability. These characteristics were due to the

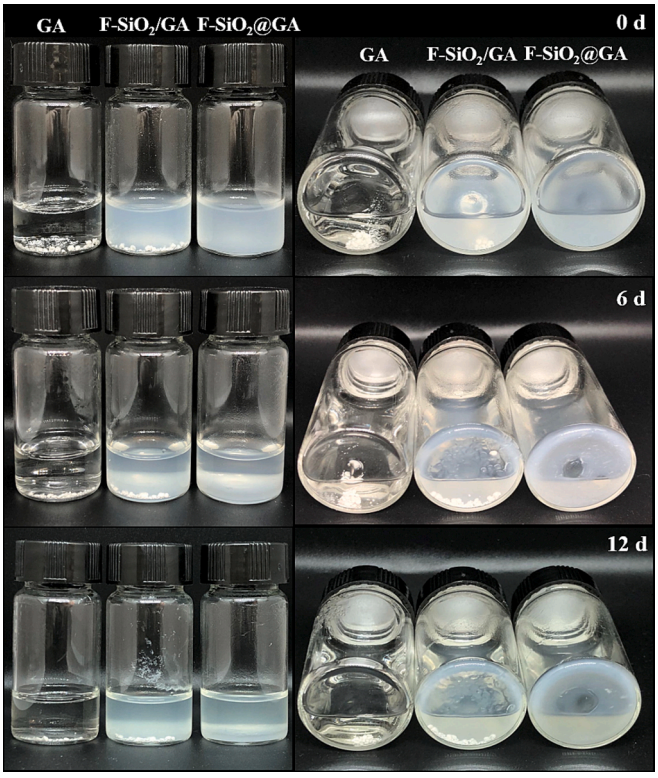

Fig. 4. Dispersion stability images of GA, F-SiO_2/GA, and F-SiO_2@GA at different storage times.

loading of GA in F-SiO_2 without affecting the surface hydrophilic properties. The experiments showed that F-SiO_2@GA prepared through solvent evaporation substantially enhanced the dispersion stability of GA in aqueous solutions.

3.2. Antioxidant activity measurements

Next, we evaluated the antioxidant capacity of GA, F-SiO_2/GA, and F-SiO_2@GA against DPPH$^{\bullet}$, $^{\bullet}OH$, and $O_2^{\bullet-}$. Fig. 5 showed that the scavenging ability of the three samples for the three types of free radicals showed concentration-dependent characteristics. Specifically, the DPPH$^{\bullet}$ scavenging rate of the three samples increased rapidly as their concentrations increased from 1 to 6 μg/mL and increased slowly when their concentration reached 6 μg/mL. However, F-SiO_2@GA showed an inhibitory ability as high as 90 % at a concentration of 8 μg/mL, indicating that GA loaded in F-SiO_2 did not lose its antioxidant activity. DPPH radical scavenging is contingent on the hydrogen-donating ability of the compounds. The IC_{50} value was selected to reflect the antioxidant strength of the different antioxidants. Low IC_{50} values indicated high free-radical scavenging activities. The IC_{50} values (DPPH$^{\bullet}$) of GA, F-SiO_2/GA, and F-SiO_2@GA were 2.910, 2.745, and 2.357 μg/mL (Fig. 5D), respectively. The $^{\bullet}OH$ scavenging curves provided in Fig. 5B illustrated that F-SiO_2@GA had higher scavenging ability than samples GA and F-SiO_2/GA ($P < 0.05$). The IC_{50} values of GA, F-SiO_2/GA, and F-SiO_2@GA for $^{\bullet}OH$ were 294.1, 333.2, and 323.8 μg/mL (Fig. 5D), respectively. The $O_2^{\bullet-}$ scavenging activity of F-SiO_2@GA was also high (Fig. 5C). The IC_{50} values of GA, F-SiO_2/GA, and F-SiO_2@GA for $O_2^{\bullet-}$ were 20.81, 12.19, and 7.042 mg/mL (Fig. 5D), respectively.

GA has limited hydrogen supply capacity due to its poor water solubility, leading to considerable impairment of its antioxidant potential in aqueous environments. F-SiO_2@GA not only improved water solubility but also improved antioxidant activity likely because GA was dispersed inside F-SiO_2 to avoid molecular accumulation, thereby inhibiting the reduced hydrogen supply capacity due to molecular aggregation.

3.3. Oxidation resistance test on GYP

Food-grade pigments have the potential to enhance the sensory attributes of food. However, food-grade pigments, such as GYP, are highly susceptible to photofading due to photo-oxidative decomposition (Tang et al., 2022a; Tang et al., 2022b). The utilization of antioxidants during food processing and storage represents an effective strategy for solving the photostability problem of food-grade pigments. Therefore, the effect of F-SiO_2@GA on the photostability of GYP was investigated. As shown in Fig. 6A, the GYP solution (CK group) experienced severe photofading after 10 h of natural light irradiation, presenting an absorbance retention rate of only 20.92 % (Fig. 6B). The GYP solutions added to GA, F-SiO_2/GA, and F-SiO_2@GA showed considerably improved photostability compared with the GYP solution added to CK group ($P > 0.05$) and exhibited retention rates of 43.55 %, 36.77 %, and 45.71 %, respectively. F-SiO_2@GA had the best ability to inhibit photofading. The phenolic group in GA could donate H-atoms to scavenge free radicals generated by pigments after light irradiation, thereby effectively inhibiting the photo-oxidation and degradation of pigments (Wu et al., 2022). Additionally, the nonpolar microenvironment within the silica

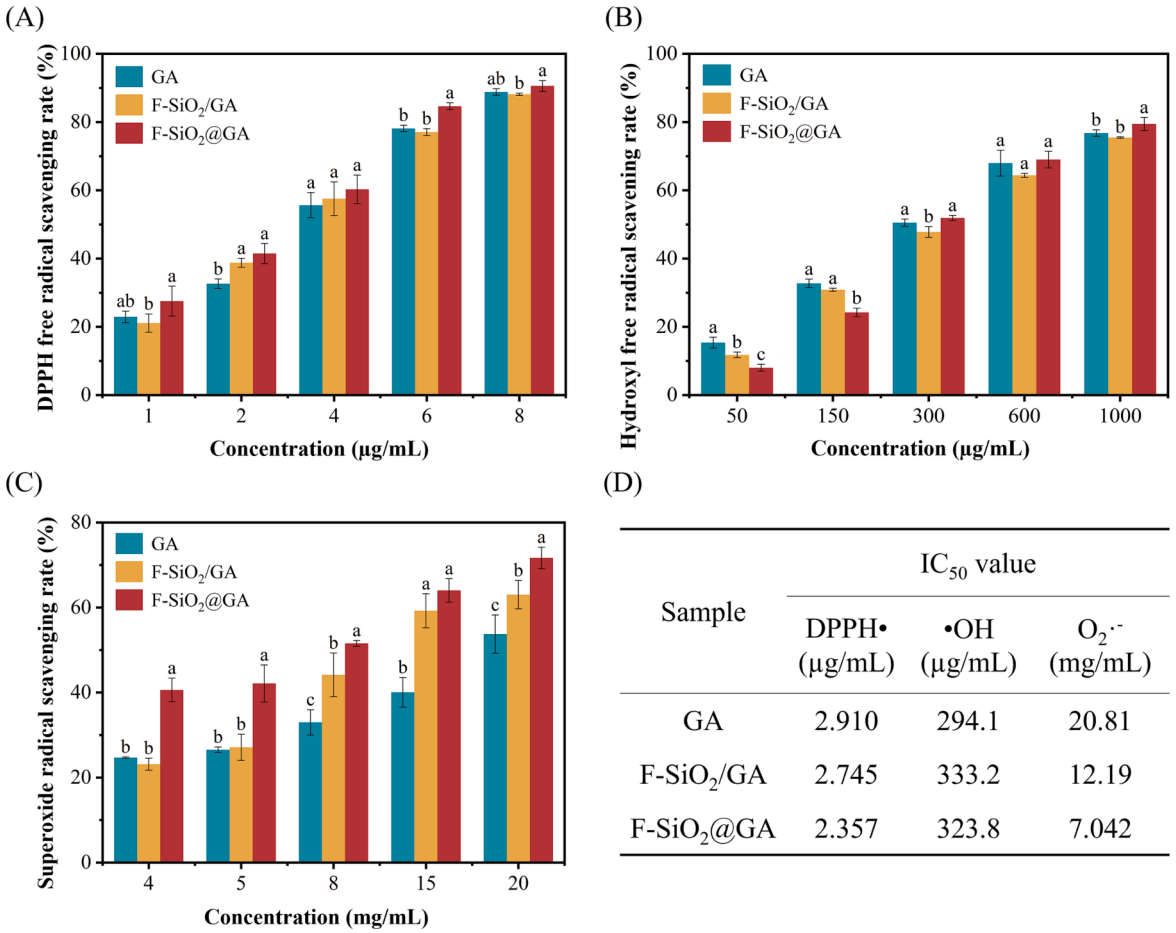

Sample	IC_{50} value		
	DPPH• (μg/mL)	•OH (μg/mL)	$O_2^{\bullet-}$ (mg/mL)
GA	2.910	294.1	20.81
F-SiO_2/GA	2.745	333.2	12.19
F-SiO_2@GA	2.357	323.8	7.042

Fig. 5. Scavenging activities for (A) DPPH, (B) $^{\bullet}OH$, and (C) $O_2^{\bullet-}$ of GA, F-SiO_2/GA, and F-SiO_2@GA. (D) IC_{50} values of GA, F-SiO_2/GA, and F-SiO_2@GA. Results are shown as mean ± SD (n = 3).

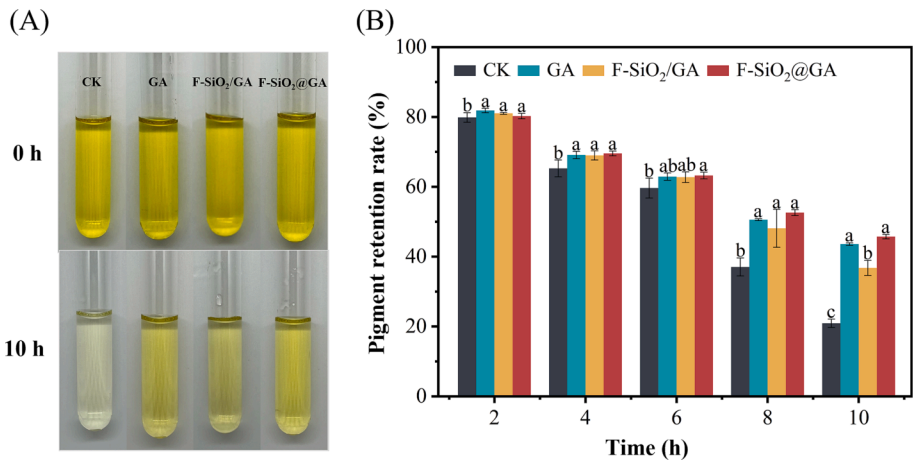

Fig. 6. (A) Preservation effect and (B) pigment retention rates of GA, F-SiO_2/GA, and F-SiO_2@GA under natural light irradiation. Results are shown as mean ± SD (n = 3).

matrix served as a protective barrier for H-atoms provided by GA, preventing their quenching by water molecules (Jiao et al., 2020). These combined factors ultimately contributed to the superior anti-photo-oxidation effect of F-SiO_2@GA on GYP.

3.4. Shrimp preservation

We subsequently assessed the overall preservation effect of F-SiO_2@GA on chilled L. *vannamei* using pH, TVBN, and TBARS values as characteristic indices to explore the multifunctional application potential of F-SiO_2@GA. It could be observed from Fig. 7A that the heads of shrimp in CK group began to show obvious red changes after 6 days of storage, which was due to the combined effect of oxidative denaturation of pigment protein and release of red pigment molecules, as well as the oxidation of astaxanthin into astaxanthin. In contrast, GA, F-SiO_2/GA, and F-SiO_2@GA could inhibit the phenomenon of shrimp head redness to a certain extent. Especially for F-SiO_2@GA, the shrimp head did not appear red after 8 days of storage, and the appearance of the whole shrimp was still slightly transparent with luster.

Fig. 7B illustrated the pH variations observed in shrimp treated with different samples during refrigeration. The initial pH value of CK group was 6.8 ± 0.03, which was consistent with previously reported findings (Chen et al., 2019). The low initial pH value (6.60 ± 0.05) observed in the treatment groups might be related to the slight acidity of GA (Wu et al., 2016). During the subsequent 8 days of storage, the pH value of CK group increased considerably faster than that of the treated groups ($P < 0.05$). The pH value of CK group approached 7.8 after 5 days, indicating that the shrimp were unsuitable for consumption (Chen et al., 2019). Endogenous enzymes and exogenous microorganisms catalyzed the breakdown of proteins, resulting in the production of alkaline substances, such as ammonia and trimethylamine, which were primarily responsible for the increase in pH levels (Olatunde et al., 2021). After 8 days of refrigeration, the pH values of each group reached 7.95, 7.88, 7.75, and 7.60. These findings indicated that the pH value of shrimp in F-SiO_2@GA treatment group was effectively controlled throughout refrigerated storage at 4 °C. The inhibitory effect on pH value could be attributed to the combined effect of protein antioxidation and partial antibacterial effects of GA (Peng et al., 2022). The TVBN values of shrimp subjected to different treatments for 8 days were presented in Fig. 7C. The initial TVBN values of the samples were 2.56 ± 0.21 mg/100 g (less than 10 mg/100 g), indicating that the raw materials were freshness (Olatunde et al., 2021). During the initial stage of storage, the TVBN values of all four sample groups gradually increased. With the extension of storage time, the rapid proliferation of microorganisms and acceleration of protein decomposition led to a rapid increase in TVBN values in each group, especially in CK group (Chaijan et al., 2020). However, the TVBN values of the shrimp in the treatment groups were considerably lower than those in CK group ($P < 0.05$). No notable difference was found between the TVBN values of the shrimp in GA and F-SiO_2/GA groups ($P > 0.05$), whereas the lowest TVBN value was

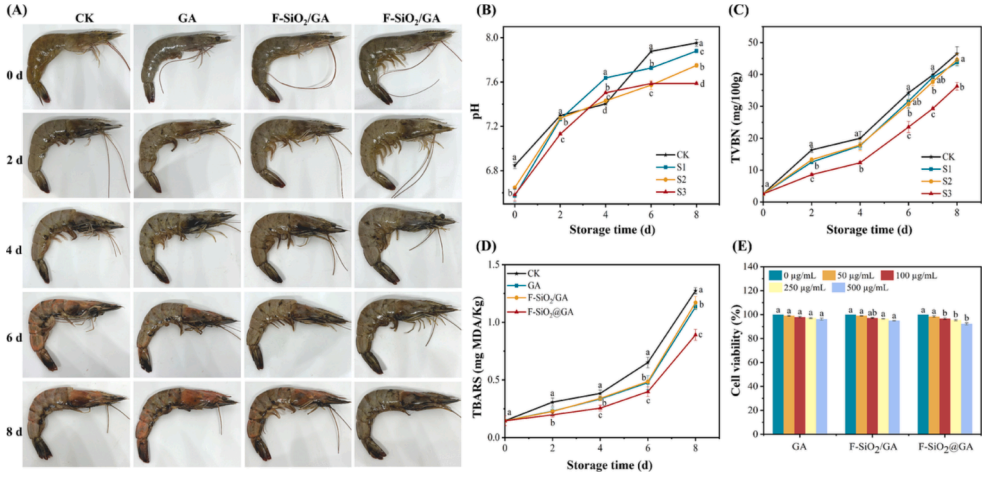

Fig. 7. Preservation effect of GA, F-SiO_2/GA, and F-SiO_2@GA on L. *vannamei* during refrigerated storage at 4 °C. (A) Visual appearance, (B) pH variations, (C) TVBN variations, (D) TBARS value, and (E) cytotoxicity on Raw264.7 macrophages cells. Results are shown as mean ± SD (n = 3).

observed in F-SiO_2@GA group ($P < 0.05$). The TVBN values of CK, GA, and F-SiO_2/GA groups on day 6 exceeded the acceptable upper limit (30–35 mg/100 g) and were 34.21, 31.65, and 30.71 mg/100 g, respectively (Chen et al., 2019). In contrast, the TVBN value of F-SiO_2@GA group remained below the permissible limit (29.03 mg/100 g) after 7 days, indicating that F-SiO_2@GA had a sustained antibacterial effect. Previous studies had reported that GA exhibited potent inhibitory activity against common foodborne pathogens and spoilage bacteria (Li et al., 2022b). Furthermore, TBARS value is an important indicator to evaluate lipid oxidation in seafood muscles (Shi et al., 2021). As shown in Fig. 7D, the TBARS value in CK group continuously increased and significantly higher than that of the treatment groups ($P < 0.05$) throughout the storage period. After 8 days of storage, F-SiO_2@GA exhibited the lowest TBARS value, indicating its remarkable capacity in scavenging free radicals. As we know, free radicals, metal ions, lipoxygenases, peroxidases, and microbial enzymes could induce lipid oxidation in aquatic products (Li et al., 2022b). Therefore, GA molecules in the nanocomposites could effectively donate electrons or hydrogen atoms to neutralize free radicals, thereby effectively terminating lipid oxidation (Ahmad Shiekh & Benjakul, 2020). As a result, the water-soluble F-SiO_2@GA effectively controlled the increase in pH, TVBN, and TBARS values to extend the shelf life of shrimp.

The cytotoxicity of the nanocomposites should be ultimately considered (Zhang et al., 2022). Therefore, the cytotoxicity of F-SiO_2@GA was assessed using Raw264.7 macrophages cells. As could be seen from Fig. 7E, the cells co-incubated with nanocomposites did not exhibit any significant cytotoxic effects, even at a high concentration of 500 μg/mL. The low toxicity of nanocomposites mainly attributed to the non-toxic properties of F-SiO_2. This was an important reason why F-SiO_2 was chosen as the carrier for GA in this study.

3.5. Strengthening mechanism of water solubility and water-based biological activity

During the preparation of F-SiO_2@GA, the introduction of GA molecules into the nanoporous channels of F-SiO_2 via thermal diffusion followed by gradual solvent evaporation resulted in a uniform and stable distribution of GA within the nanoporous channels (Fig. 8). The absence of π–π accumulation in the nanoporous channels allowed the exposure of phenol hydroxyl groups, increasing the number of active phenol hydroxyl groups. Based on its photosensitization ability, GYP underwent a transition and intersystem crossing under light irradiation to generate a triple excited state (T_1). Through the type I mechanism, the excited pigments donated electrons or hydrogen atoms to surrounding O_2 molecules, leading to the formation of oxygen-containing free radicals that were rapidly quenched by GA. The water-soluble F-SiO_2@GA exhibited strong permeability, effectively protecting the protein and fat of shrimp from free radical oxidation. This effect, in conjunction with the antibacterial properties of GA, effectively prolonged the preservation period of fresh shrimp.

4. Conclusions

F-SiO_2@GA was successfully prepared through solvent evaporation. SEM, DSC, FT-IR, and UV–Vis characterization techniques revealed that in F-SiO_2@GA, active GA molecules were loaded into the nanopores of F-SiO_2. The GA molecules inside F-SiO_2 exhibited distinct shifts in their morphological characteristics, displaying a uniform distribution and transitioning from a crystalline state to an amorphous form. Furthermore, the water solubility of F-SiO_2@GA considerably increased. This effect further enhanced the antioxidant activity in vitro because the active phenolic hydroxyl groups of the uniformly loaded GA were effectively exposed. In the application experiment on pigment

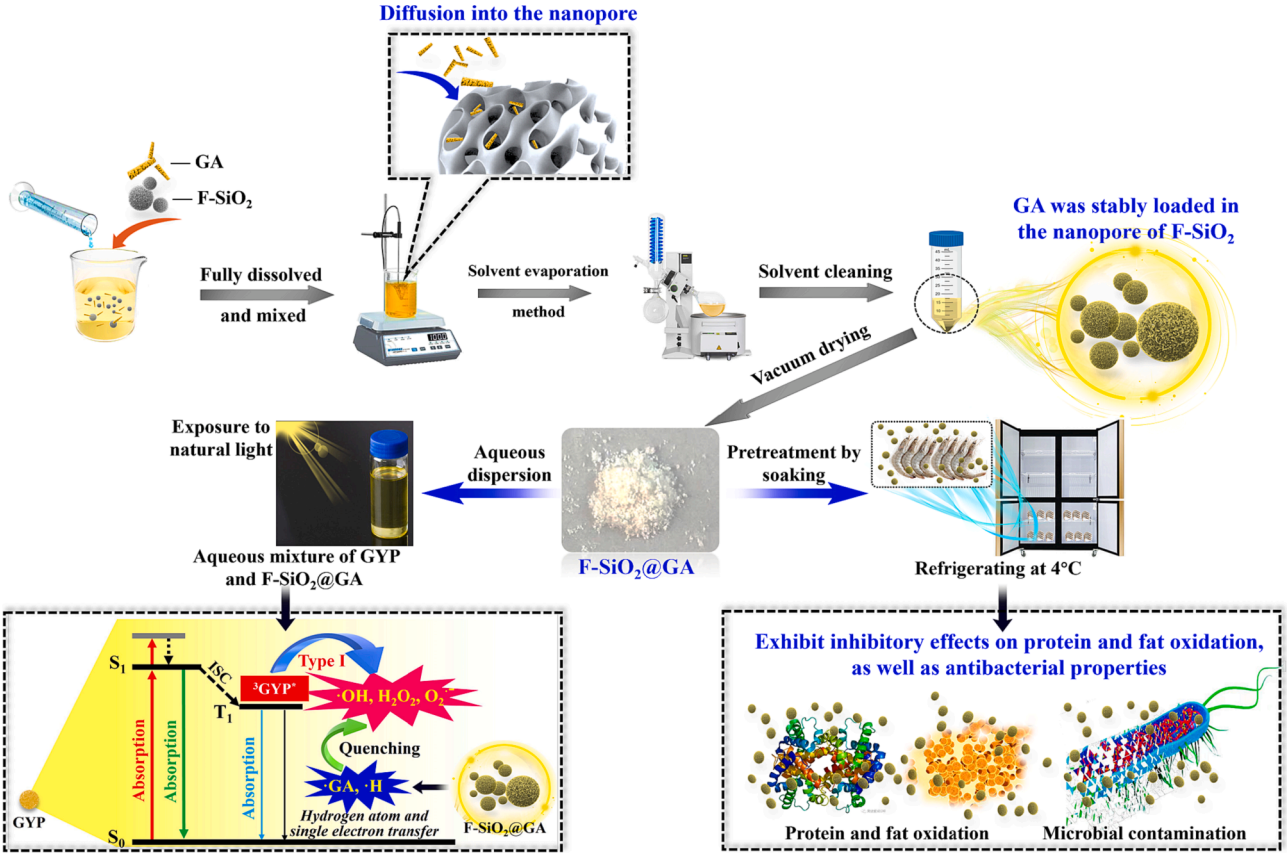

Fig. 8. Preparation of F-SiO_2@GA via solvent evaporation and its strengthening mechanism of water solubility and water-based biological activity.

antioxidants, the addition of F-SiO_2@GA effectively mitigated the photodegradation of GYP in solution states. Furthermore, in the experiment on fresh shrimp refrigeration, treatment with F-SiO_2@GA outperformed that with CK in controlling the freshness indicators pH, TVBN and TBARS values. The enhancement in the water-based biological activities of F-SiO_2@GA was attributed to the presence of GA in the non-π–π aggregation state, which exposed active phenol hydroxyl groups and further enhanced antioxidant activities. Moreover, owing to the strong hydrophilicity of F-SiO_2, the nanocomposites could effectively interact with pigment or fresh shrimp, leading to further improvement in their bioactive function. The strategy of loading bioactive molecules in F-SiO_2 presented a novel approach for enhancing the antioxidant or antibacterial properties of natural bioactive compounds.

CRediT authorship contribution statement

Huizhen Feng: Data curation, Validation, Writing – original draft. **Long Jiao:** Funding acquisition, Project administration, Writing – review & editing. **Xiaoye Zhang:** Writing – review & editing. **Soottawat Benjakul:** Data curation, Validation, Validation. **Bin Zhang:** Validation.

Declaration of competing interest

The authors declare that they have no known competing financial interests or personal relationships that could have appeared to influence the work reported in this paper.

Data availability

Data will be made available on request.

Acknowledgments

This research was supported by Zhejiang Provincial Natural Science Foundation of China under Grant No. LQ22C200011, National Natural Science Foundation of China under Grant No. U23A20263, and Special Fund for Introduced Talent to Initiate Scientific Research of Zhejiang Ocean University under Grant No. JX6311130523. The authors want to thank Shiyanjia Lab (www.shiyanjia.com) for the SEM, FT-IR, and DSC analysis. And the authors also thank Enago (www.enago.cn) for its linguistic assistance during the preparation of this manuscript.

References

Abbasi, E., Basiri, S., Shekarforoush, S. S., & Gholamhosseini, A. (2023). The efficacy of tragacanth gel incorporated with cell-free supernatants of *Lactobacillus sakei* and *Lactobacillus curvatus* for preserving Pacific white shrimp. *Food Control, 150*, Article 109781. https://doi.org/10.1016/j.foodcont.2023.109781

Ahmad Shiekh, K., & Benjakul, S. (2020). Melanosis and quality changes during refrigerated storage of Pacific white shrimp treated with chamuang (Garcinia cowa Roxb.) leaf extract with the aid of pulsed electric field. *Food Chemistry, 309*, Article 125516. https://doi.org/10.1016/j.foodchem.2019.125516

Aydogdu, A., Yildiz, E., Aydogdu, Y., Sumnu, G., Sahin, S., & Ayhan, Z. (2019). Enhancing oxidative stability of walnuts by using gallic acid loaded lentil flour based electrospun nanofibers as active packaging material. *Food Hydrocolloids, 95*, 245–255. https://doi.org/10.1016/j.foodhyd.2019.04.020

Chaijan, S., Panpipat, W., Panya, A., Cheong, L. Z., & Chaijan, M. (2020). Preservation of chilled Asian sea bass (Lates calcarifer) steak by whey protein isolate coating containing polyphenol extract from ginger, lemongrass, or green tea. *Food Control, 118*, Article 107400. https://doi.org/10.1016/j.foodcont.2020.107400

Chen, K., Shao, L. L., Huo, Y. F., Zhou, J. M., Zhu, Q., Hider, R. C., & Zhou, T. (2019). Antimicrobial and antioxidant effects of a hydroxypyridinone derivative containing an oxime ether moiety and its application in shrimp preservation. *Food Control, 95*, 157–164. https://doi.org/10.1016/j.foodcont.2018.08.008

Chen, X., Partheniadis, I., Nikolakakis, I., & Al-Obaidi, H. (2020). Solubility improvement of progesterone from solid dispersions prepared by solvent evaporation and co-milling. *Polymers, 12*(4), 854. https://doi.org/10.3390/polym12040854

Cui, Y., Wang, X., Cheng, M., Guo, Y., & Zhang, R. (2023). Controlled release mechanism of thymol loaded into mesoporous silica nanoparticles for active packaging films. *Food Bioscience, 56*, Article 103229. https://doi.org/10.1016/j.fbio.2023.103229

Dong, W., Su, J., Chen, Y., Xu, D., Cheng, L., Mao, L., Gao, Y., & Yuan, F. (2022). Characterization and antioxidant properties of chitosan film incorporated with modified silica nanoparticles as an active food packaging. *Food Chemistry, 373*, Article 131414. https://doi.org/10.1016/j.foodchem.2021.131414

Eren, Z. S., Tunçer, S., Gezer, G., Yildirim, L. T., Banerjee, S., & Yilmaz, A. (2016). Improved solubility of celecoxib by inclusion in SBA-15 mesoporous silica: Drug loading in different solvents and release. *Microporous and Mesoporous Materials, 235*, 211–223. https://doi.org/10.1016/j.micromeso.2016.08.014

He, Y., Liang, S., Long, M., & Xu, H. (2017). Mesoporous silica nanoparticles as potential carriers for enhanced drug solubility of paclitaxel. *Materials Science and Engineering: C, 78*, 12–17. https://doi.org/10.1016/j.msec.2017.04.049

Hu, J., Xu, R., Hu, J., & Deng, W. (2022). Dual stabilization of Pickering emulsion with epigallocatechin gallate loaded mesoporous silica nanoparticles. *Food Chemistry, 396*, Article 133675. https://doi.org/10.1016/j.foodchem.2022.133675

Huang, Z., Wang, Q., Cao, J., Zhou, D., & Li, C. (2023). Mechanisms of polyphenols on quality control of aquatic products in storage: A review. *Food Science and Nutrition, 1–20*. https://doi.org/10.1080/10408398.2023.2167803

Jiao, L., Liu, Y., Zhang, X., Hong, G., Zheng, J., Cui, J., Peng, X., & Song, F. (2020). Constructing a local hydrophobic cage in dye-doped fluorescent silica nanoparticles to enhance the photophysical properties. *ACS Central Science, 6*(5), 747–759. https://doi.org/10.1021/acscentsci.0c00071

Li, B., Hu, Y., Wu, T., Feng, Y., Jiang, C., Du, H., & Lu, S. (2022a). Apigenin-oxymatrine binary co-amorphous mixture: Enhanced solubility, bioavailability, and anti-inflammatory effect. *Food Chemistry, 373*, Article 131485. https://doi.org/10.1016/j.foodchem.2021.131485

Li, J., Yang, Y., Li, Y., Zhao, P., Fei, J., & Xie, Y. (2023). Detection of gallic acid in food using an ultra-sensitive electrochemical sensor based on glass carbon electrode modified by bimetal doped carbon nanopolyhedras. *Food Chemistry, 429*, Article 136900. https://doi.org/10.1016/j.foodchem.2023.136900

Li, Q., Zhou, W., Zhang, J., Zhu, J., Sun, T., Li, J., & Cheng, L. (2022b). Synergistic effects of ε-polylysine hydrochloride and gallic acid on *Shewanella putrefaciens* and quality of refrigerated sea bass fillets. *Food Control, 139*, Article 109070. https://doi.org/10.1016/j.foodcont.2022.109070

Liu, J. (2021a). The preservation effects of chitosan copolymers (gallic acid and protocatechuic acid) on sea bass (Lateolabrax japonicus) fillets. *Aquaculture and Fisheries, 8*(3), 305–315. https://doi.org/10.1016/j.aaf.2021.09.009

Liu, W., Xie, J., Li, L., Xue, B., Li, X., Gan, J., Shao, Z., & Sun, T. (2021b). Properties of phenolic acid-chitosan composite films and preservative effect on *Penaeus vannamei*. *Journal of Molecular Structure, 1239*, Article 130531. https://doi.org/10.1016/j.molstruc.2021.130531

Olatunde, O. O., Tan, S. L. D., Shiekh, K. A., Benjakul, S., & Nirmal, N. P. (2021). Ethanolic guava leaf extracts with different chlorophyll removal processes: Anti-melanosis, antibacterial properties and the impact on qualities of Pacific white shrimp during refrigerated storage. *Food Chemistry, 341*, Article 128251. https://doi.org/10.1016/j.foodchem.2020.128251

Othón-Díaz, E. D., Fimbres-García, J. O., Flores-Sauceda, M., Silva-Espinoza, B. A., López-Martínez, L. X., Bernal-Mercado, A. T., & Ayala-Zavala, J. F. (2023). Antioxidants in oak (Quercus sp.): Potential application to reduce oxidative rancidity in foods. *Antioxidants, 12*(4), 861. https://doi.org/10.3390/antiox12040861

Peng, Z., Li, Y., Tan, L., Chen, L., Shi, Q., Zeng, Q. H., Liu, H., Wang, J. J., & Zhao, Y. (2022). Anti-tyrosinase, antioxidant and antibacterial activities of gallic acid-benzylidenehydrazine hybrids and their application in preservation of fresh-cut apples and shrimps. *Food Chemistry, 378*, Article 132127. https://doi.org/10.1016/j.foodchem.2022.132127

Petcu, C. D., Mihai, O. D., Tăpăloagă, D., Gheorghe-Irimia, R. A., Pogurschi, E. N., Militaru, M., Borda, C., & Ghimpețeanu, O. M. (2023). Effects of plant-based antioxidants in animal diets and meat products: A review. *Foods, 12*(6), 1334. https://doi.org/10.3390/foods12061334

Rahaman, S. N., Ayyadurai, N., & Anandasadagopan, S. K. (2023). Synergistic effect of vancomycin and gallic acid loaded MCM-41 mesoporous silica nanoparticles for septic arthritis management. *Journal of Drug Delivery Science and Technology, 82*, Article 104353. https://doi.org/10.1016/j.jddst.2023.104353

Shi, R., Li, Y., & Liu, L. (2021). Synergistic anti-oxidative and antimicrobial effects of oat phenolic compounds and ascorbate palmitoyl on fish balls during cold storage. *Journal of Food Science, 86*(10), 4628–4636. https://doi.org/10.1111/1750-3841.15922

Song, Y., Huang, H., He, D., Yang, M., Wang, H., Zhang, H., Li, J., Li, Y., & Wang, C. (2021). Gallic acid/2-hydroxypropyl-*β*-cyclodextrin inclusion complexes electrospun nanofibrous webs: Fast dissolution, improved aqueous solubility and antioxidant property of gallic acid. *Chemical Research in Chinese Universities, 37*(3), 450–455. https://doi.org/10.1007/s40242-021-0014-0

Tang, L., Liu, H., Huang, G., Yuan, Z., Fu, M., Bu, Z., Wen, J., & Xu, Y. (2022a). The structural characterization, physicochemical properties, and stability of gardenia yellow pigment microcapsules. *LWT, 162*, Article 113507. https://doi.org/10.1016/j.lwt.2022.113507

Tang, L., Liu, H., Huang, G., Yuan, Z., Fu, M., Wen, J., Yu, Y., Hu, T., & Xu, Y. (2022b). The physicochemical properties and immunomodulatory activities of gardenia yellow pigment from gardenia fruit. *Journal of Functional Foods, 93*, Article 105096. https://doi.org/10.1016/j.jff.2022.105096

Wang, H., You, S., Wang, W., Zeng, Y., Su, R., Qi, W., Wang, K., & He, Z. (2022). Laccase-catalyzed soy protein and gallic acid complexation: Effects on conformational structures and antioxidant activity. *Food Chemistry, 375*, Article 131865. https://doi.org/10.1016/j.foodchem.2021.131865

Wianowska, D., & Olszowy-Tomczyk, M. (2023). A concise profile of gallic acid—from its natural sources through biological properties and chemical methods of

determination. *Molecules, 28*(3), 1186. https://doi.org/10.3390/molecules28031186

Wu, C., Fu, S., Xiang, Y., Yuan, C., Hu, Y., Chen, S., Liu, D., & Ye, X. (2016). Effect of chitosan gallate coating on the quality maintenance of refrigerated (4°C) silver pomfret (Pampus argentus). *Food and Bioprocess Technology, 9*(11), 1835–1843. https://doi.org/10.1007/s11947-016-1771-5

Wu, J., Wang, X., He, Y., Li, J., Ma, K., Zhang, Y., Li, H., Yin, C., & Zhang, Y. (2022). Stability evaluation of gardenia yellow pigment in presence of different phenolic compounds. *Food Chemistry, 373*, Article 131441. https://doi.org/10.1016/j.foodchem.2021.131441

Zhang, G., Zheng, C., Huang, B., & Fei, P. (2020). Preparation of acylated pectin with gallic acid through enzymatic method and their emulsifying properties, antioxidation activities and antibacterial activities. *International Journal of Biological Macromolecules, 165*, 198–204. https://doi.org/10.1016/j.ijbiomac.2020.09.195

Zhang, W., Ezati, P., Khan, A., Assadpour, E., Rhim, J. W., & Jafari, S. M. (2023). Encapsulation and delivery systems of cinnamon essential oil for food preservation applications. *Advances in Colloid and Interface Science, 318*, Article 102965. https://doi.org/10.1016/j.cis.2023.102965

Zhang, Y., Dong, L., Liu, L., Wu, Z., Pan, D., & Liu, L. (2022). Recent advances of stimuli-responsive polysaccharide hydrogels in delivery systems: A Review. *Journal of Agricultural and Food Chemistry, 70*(21), 6300–6316. https://doi.org/10.1021/acs.jafc.2c01080

Zhao, Y., Guo, G., Xu, B., Liu, H., Tian, H., Li, J., Ouyang, Y., Xiang, A., & Kumar, R. (2023). Electrospun natural polypeptides based nanofabrics enriched with antioxidant polyphenols for active food preservation. *Food Chemistry, 405*, Article 134991. https://doi.org/10.1016/j.foodchem.2022.134991